JOURNAL OF APPLIED ELECTROCHEMISTRY **27** (1997) 335–344

Electrochemical and ellipsometric study of the oxide films formed on copper in borax solution Part I: Effect of oxygen

J. O. ZERBINO, M. F. L. DE MELE

Instituto de Investigaciones Fisicoquimicas Teoricas y Aplicadas (INIFTA), Facultad de Ciencias Exactas, Universidad Nacional de La Plata, Sucursal 4, Casilla de Correo 16, 1900 La Plata, Argentina

Received 10 January 1996; revised 29 May 1996

The formation and reduction of passive layers on copper in weakly alkaline solutions saturated with N_2 and O_2 were studied. Voltammetric and ellipsometric techniques were employed to examine the structural characteristics of the layers formed in the −0.32 to 0.75 V vs RHE potential region. Optical measurements at open circuit potentials (E_{oc}) were also made to simulate operational conditions. The passive layer consists of a duplex structure: an outer hydrated copper oxide film and an inner dehydrated film. This inner layer is composed of Cu_2O with a surface excess of Cu(II) ions. The growth rate of the oxide layers at controlled potentials is higher in O_2 saturated solution. The corrosion resistance of copper depends on the presence of O_2 in the electrolyte, on the stirring rate and on the E_{oc} value.

1. Introduction

Stator windings of turbo generators are water cooled and cooling efficiency is affected by the corrosion of the copper components. At low O_2 concentration (20 μg dm^{-3}) many of the oxide nuclei are swept along by the flow and accumulate on filters and downstream hydraulic discontinuities. Aeration was reported as an efficient way to control corrosion by pure water [1]. However, the O_2 role is not clearly understood.

Films formed in deaerated sol under potentiostatic conditions have a duplex structure, probably an inner layer grown by a solid state mechanism and an outer layer formed by precipitation of a supersaturated sol [2–7]. Under these experimental conditions the $Cu(OH)_2$ [2] and Cu_2O layer [6] are suggested as the major barrier for the ion migration. Studies made using sol in contact with oxygen/helium mixtures (1% and 10% in O_2) as well as pure O_2 atmospheres, showed that the chemical composition of the film, its structural characteristics, morphology and thickness depend on the water O_2 content [8].

Different Cu(I) and Cu(II) species formed on copper have been evaluated by ex situ analysis. However, the depth profile of the passive layer obtained by ISS does not necessarily demonstrate the composition of the layers (CuO, $Cu(OH)_2$ or Cu_2O). $Cu(OH)_2$ may be dehydrated and changed during ion bombardment [2]. On the other side, the structure of the oxides formed under polarization may be different from that obtained in practice under open circuit conditions.

Notwithstanding the vast literature on copper corrosion, the interfacial processes involving soluble and adsorbed species are still under discussion. This work examines the formation and reduction of passive layers on copper in borax sol saturated with N_2 and O_2. *In situ* voltammetric and ellipsometric measurements were employed at controlled potentials to complement the available information. Optical measurements were also made under open circuit condition to simulate operational performance.

2. Experimental details

A 99.9% pure copper disc working electrode of 0.40 cm^2 apparent area, a Pt foil auxiliary electrode and a reference hydrogen electrode were assembled in a conventional cell for ellipsometric measurements [9]. Potentials are referred to the reversible hydrogen electrode (RHE) scale in the same sol. The electrolyte sol, a borax buffer pH 9.0, was prepared from $Na_2B_2O_7$ 0.075 M, H_3BO_3 0.15 M Mallinckrodt p.a. and MilliQ* water. The working electrode was mirror polished with 0.3 and 0.05 μm alumina, then rinsed with MilliQ* water and finally immersed in the cell. The ellipsometer (Rudolph Research type 437002/200 E) was used in the null mode, with the incident light beam at 70° and the azimuthal angle (compensator) set at 135°. The wave length employed was $\lambda = 546.1$ nm. Runs were made at room temperature under N_2 (sol I) and O_2 bubbling (sol II). The refraction indices of the substrate ($n - i\,k$) were obtained using the polished copper electrode held at a cathodic potential $E_c = -0.32$ V. The resulting values are in good agreement with previously reported data [7, 9–11].

0021-891X

The experimental procedure was the following. First, the ellipsometric parameters of the initial recently polished Cu surface were obtained at $E_c = -0.32$ V.

Procedure I: The values of Δ and Ψ were measured at open circuit potentials (E_{oc}) in sol I or sol II.

Procedure II: An anodic scan at either $v = 0.01$ V s^{-1} or $v = 0.10$ V s^{-1} from E_c up to an anodic potential limit E_a followed by a potential holding at E_a was made in sol I to obtain Δ and Ψ values during the growth of the oxide layers.

Procedure III: Experiments were made in sol I. After different times at either E_{oc} (procedure I) or at E_a (procedure II), the potential was negatively scanned at 0.01 V s^{-1} from these potentials to E_c. Finally, the ellipsometric parameters were measured at $E_c = -0.32$ V.

Procedure IV: Δ, Ψ and the current i were simultaneously measured during a potentiodynamic cycle from E_c to $E_a = 0.68$ V at 1.5 mV s^{-1}.

3. Results:

3.1. *Oxides formed at* E_{oc}

3.1.1. Ellipsometric measurements. The oxide formation on copper immersed in borax buffer sol either I or II was evaluated at open circuit for a 24 h period. The Δ/Ψ plot for stirred sol I (Fig. 1 A) shows a steady decrease of Δ while Ψ increases (about six and two degrees, respectively). In the case of sol II the Δ/Ψ relationship is more complex than in case of Fig. 1 A. In a stagnant sol the change in Ψ is smaller than in a stirred sol (Fig. 1B and 1C).

The time dependence of Δ values of Fig. 1 and the corresponding open circuit potential E_{oc} are plotted in Fig. 2. In sol I (Fig. 2, curve a) E_{oc} rises to 0.37 V during the first minutes and after 30 min attains a stable value of 0.540 V. The change in Δ ($-\delta\Delta$) in-

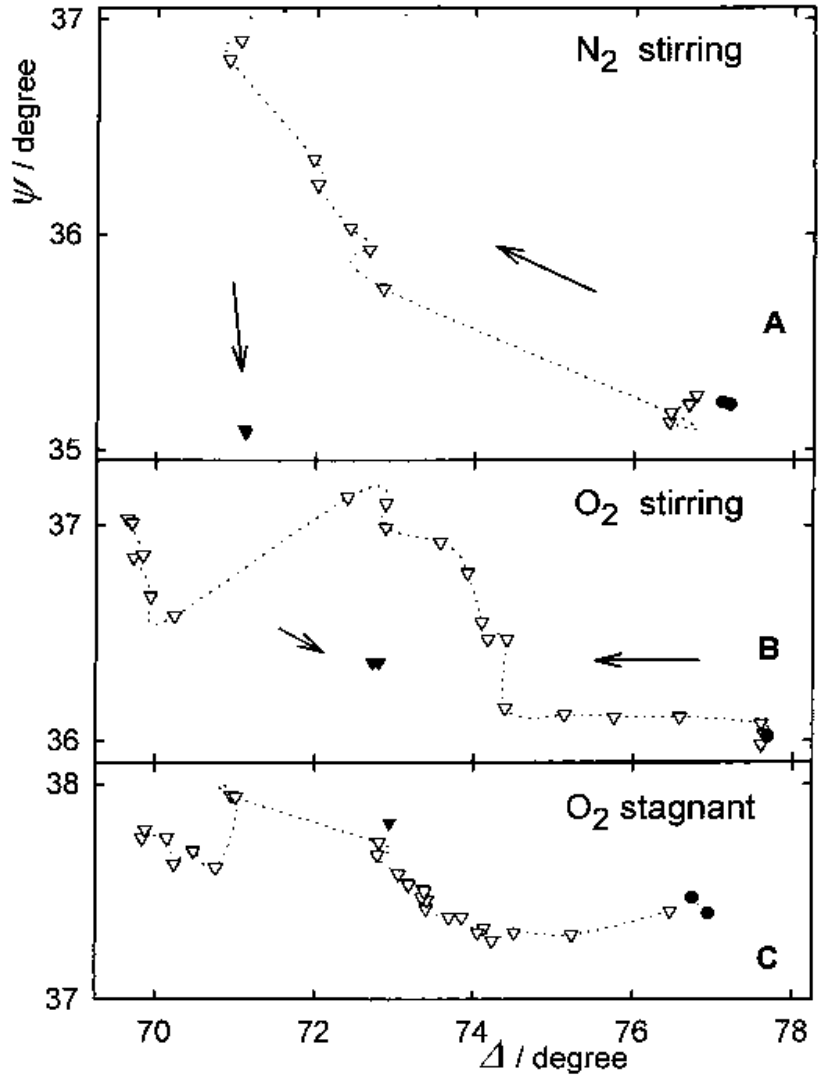

Fig. 1. Evolution of the ellipsometric parameters Δ/Ψ in borax sol, pH 9.0: (●) at $E_c = -0.32$ V; (▽) at E_{oc} and (▼) at E_c after the reduction scan: (A) N_2 sol, (B) and (C) O_2 sol.

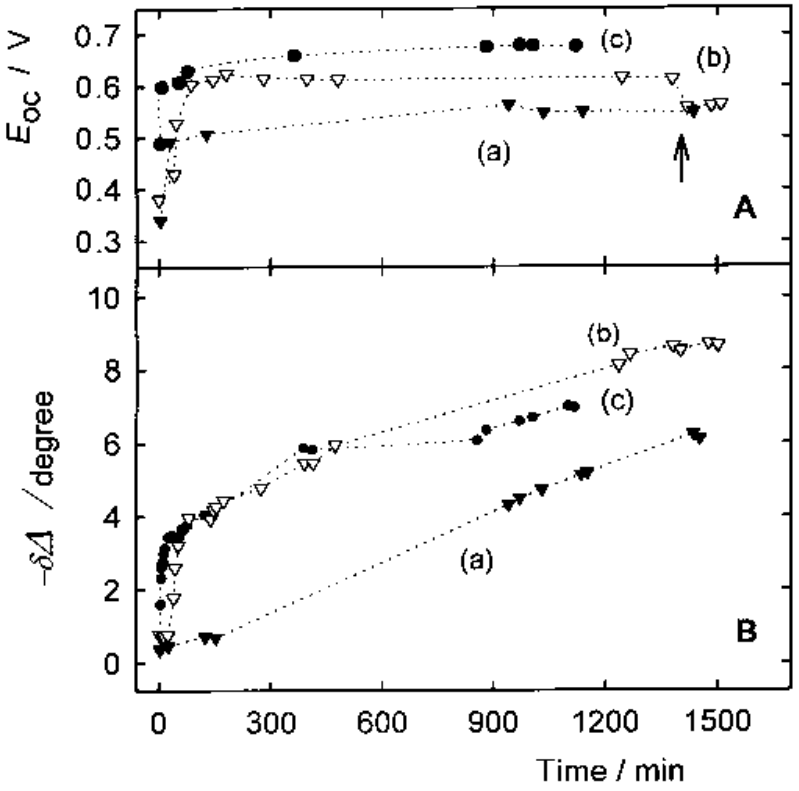

Fig. 2. Dependence of Δ and E_{oc} on time from Fig. 1: a (▼) N_2 sol, b (▽) O_2 stirring sol, c (●) O_2 stagnant sol.

itially shows a small step of about 0.2 degree and then grows linearly with time.

In sol II E_{oc} reaches 0.64 V after 10 min (Fig. 2A, curves b and c). The $-\delta\Delta/t$ dependence shows a parabolic law (Fig. 2B, curves b and c). After the initial growth, $-\delta\Delta$ shows a linear law with time similar to that observed in sol I (Fig. 2B, curve a). E_{oc} decreases from 0.60 to 0.54 V when O_2 is removed by N_2 bubbling (Fig. 2A curve b, see arrow at $t = 1400$ min). No change in Δ and Ψ was observed simultaneously with the E_{oc} decrease. In the case of stagnant oxygenated sol the behaviour is similar to that corresponding to stirred sol. However, the E_{oc} is more anodic and the increase in Ψ is smaller than that observed in stirred oxygenated sol (Fig. 1B and C and 2A, curves b and c).

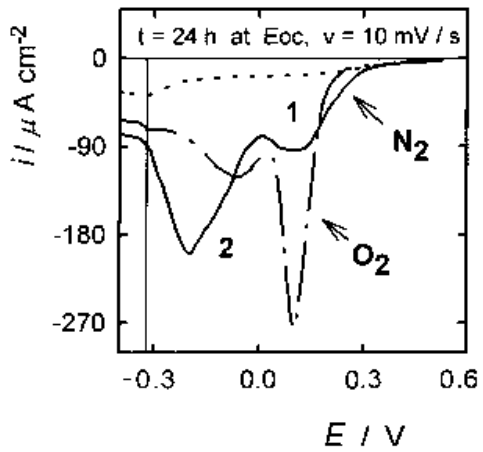

Fig. 3. First negative going scan to electroreduce the oxide layers after 24 h at E_{oc} under O_2 bubbling (dashed point line), 24 h at E_{oc} under N_2 bubbling (solid line), 3 h at E_{oc} under N_2 bubbling (dotted line). Transient current at E_c are recorded on the left.

3.1.2. Potentiodynamic reduction. Figure 3 shows the *i*/*E* relationship recorded when a 24 h old oxide layer, spontaneously formed, was reduced during a cathodic scan from $E_a = E_{oc}$ to $E_c = -0.32$ V (procedure III). The voltammogram corresponding to sol II shows two peaks: one more anodic and higher at 0.09 V (peak 1) and a smaller and broader peak at −0.06 V (peak 2). In sol I peak 1 is lower than peak 2 which is larger and more cathodic than that corresponding to sol II. The charges (Q) involved in the cathodic voltammograms are about 5600 μC cm^{-2} and 6600 μC cm^{-2} for sol II and sol I, respectively. In experiments made after 48 h at E_{oc} similar current contributions and a linear Q/t dependence resulted.

The ellipsometric parameters measured at E_c after the cathodic scan are different from those measured at the beginning of the experiment (Fig. 1). The *i*/*E* relationship associated with the reduction of the oxide layer formed during 3 h at E_{oc} in sol I is also included in Fig. 3 as a reference. It shows a contribution related to hydrogen reduction and a small one at 0.09 V visible at higher scale.

3.2. *Oxides formed at constant potential*

3.2.1. Ellipsometric measurements in deaerated sol. Figure 4 shows Δ and Ψ values when the potential is held at different anodic limits $E_a = 0.70$, 0.65 or 0.56 V (procedure II at $v = 0.10$ V s^{-1}). $-\delta\Delta$ was

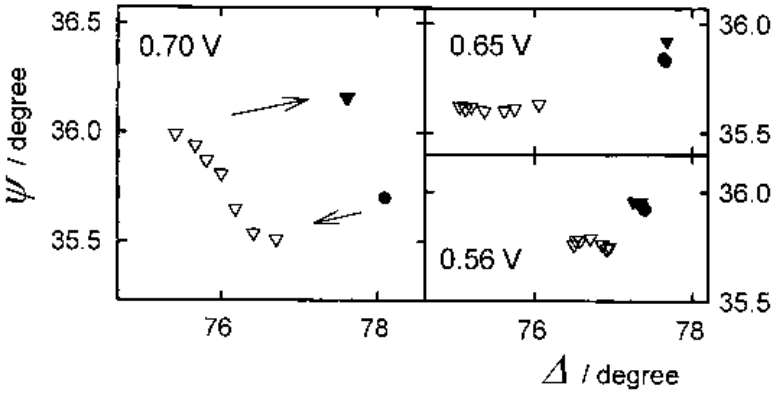

Fig. 4. Δ and Ψ evolution with time at different E_a. Measurements were made at $E_c = -0.32$ V (●), at E_a (▽) for 20 min and (▼) at E_c after reduction. E_a values are indicated in each plot.

higher at more anodic E_a. At E_a lower than 0.70 V the Δ/Ψ values measured after the oxide reduction at 0.10 V s^{-1} (filled inverted triangles) are close to the Δ/Ψ values corresponding to the bare surface (filled circles). In contrast, after 3 or 4 min at $E_a = 0.7$ V a significant increase in Ψ is observed that remains after the reduction process.

The time dependence of the optical data plotted in Fig. 4 is shown in Fig. 5. Additional measurements at $E_a = 0.75$ V are also included. Potential holdings at $E_a = 0.56$ V and $E_a = 0.65$ V show that there is an initial $-\delta\Delta$ of about 0.3 and 1.2 degrees, respectively. Then, a linear and a parabolic dependence of $-\delta\Delta$ against time are observed respectively. For $E_a = 0.70$ V and $E_a = 0.75$ V three regions can be distinguished: Region A: (includes the first 3 min) the initial $\delta\Psi$ (−0.2 degree) was similar to that obtained for lower E_a; Region B: (from 3 min to 9 min in the case of 0.75 V and up to 14 min for 0.70 V) low $-\delta\Delta/t$ and high $\delta\Psi/t$ slopes were observed; Region C: (from 9 to 20 min for 0.75 V and from 14 to 20 min for 0.70 V) the $\delta\Psi/t$ slopes are lower and the $-\delta\Delta/t$ slopes are higher than in region B. In region A and B for $E_a = 0.70$ V and $E_a = 0.75$ V the $-\delta\Delta$ is lower than that observed for $E_a = 0.65$ V. The decrease in the $\delta\Psi/t$ slope correlates with the increase in the $-\delta\Delta/t$ slope.

3.2.2. Electroreduction of the oxide layer. After holding the potential at E_a for 20 min the oxide layers were electroreduced at 0.10 V s^{-1} according to procedure III. The cathodic scan from $E_a = 0.543$ V to E_c shows two current contributions: 1 and 1′, (Fig. 6). For $E_a = 0.618$ V, an increase in charge and also a shift of the initial profile in the cathodic direction are observed. However, a further increase in E_a (0.700 V) shifts the cathodic peak anodically.

3.2.3. Ellipsometric and voltammetric parameters in sol I. In Fig. 7 relationships between the following parameters are shown: the anodic potential E_a; $-\delta\Delta$ between the bare surface and after 20 min at E_a; the potential of the reduction peak, E_p and the cathodic charges involved in the cathodic sweep. QI and QII

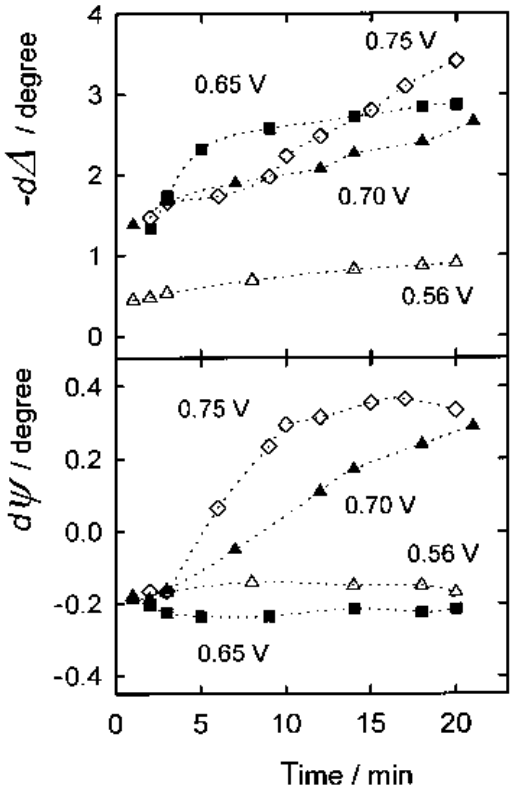

Fig. 5. Evolution of $-\delta\Delta$ and $\delta\Psi$ with time at different E_a indicated on each curve.

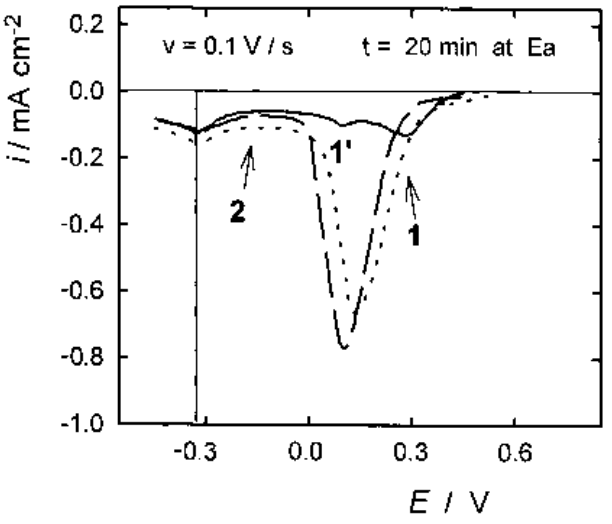

Fig. 6. First cathodic scan starting at E_a after a potential holding for 20 min at this potential (procedure II). E_a: (—) 0.543, (— —) 0.618 and (- - - -) 0.700 V.

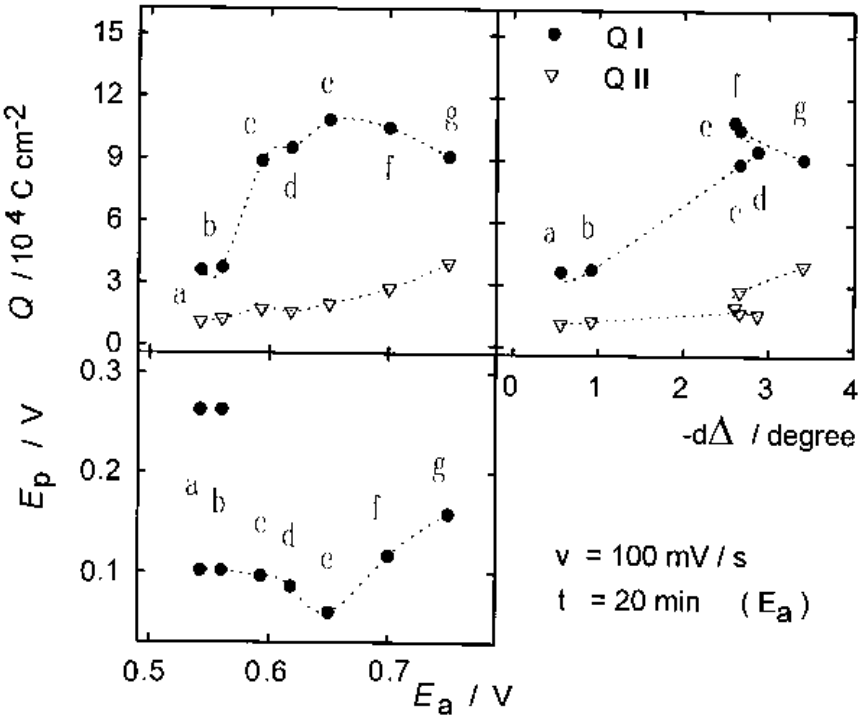

Fig. 7. Dependence of the cathodic reduction charge Q, the peak potential E_p and Δ on E_a after a potential holding for $t = 20$ min at E_a.

are the charges corresponding to the potential regions from E_a to 0.01 V and from 0.01 V to E_c respectively. E_p shows a shift in the cathodic direction when E_a increases up 0.65 V (points a–e) and to the anodic direction for more anodic E_a values (points f–g). The cathodic charge QI is higher when E_a is more anodic, reaching a maximun at $E_a = 0.65$ V (point e). The $-\delta\Delta$ against QI plot shows a linear relationship from $E_a = 0.54$ V to 0.59 V (points a–d) while QII remains constant. For E_a values between 0.59 and 0.70 V (points c–f) there is a small increase in the total charge without modifications in the $-\delta\Delta$ value. A further increase in E_a shows an increase in $-\delta\Delta$, a decrease in QI and an increase in QII.

Results of Figs 4 and 5 are summarized in Fig. 8. Additional data for different anodic potential limits E_a are included. $-\delta\Delta$ and $\delta\Psi$ measured after 20 min at E_a are plotted against E_a. These results show that the $-\delta\Delta$ values are practically independent of the anodic sweep rate for potentials up to 0.65 V. The $-\delta\Delta$ against E_a plot shows three regions (Fig. 8). In the first region up to $E_a = 0.53$ V there is a small change in Δ and Ψ. The second region between 0.53 V and 0.63 V shows a linear dependence between $-\delta\Delta$ and E_a. The third region for E_a equal to or more anodic than 0.63 V shows several phenomena: (i) after 20 min of potential holding $-\delta\Delta$ shows a maximun at $E_a = 0.63$ V; (ii) Ψ remains nearly constant up to 0.65 V and then suddenly increases; (iii) the decrease in $-\delta\Delta$ in the region 0.63/0.65 V is related to a small increase in QI (points d, e, f, Fig. 7). After a short period at E_a (1 min) the $-\delta\Delta$ against E_a values were two times lower in regions 2 and 3 than those of Fig. 8A and Ψ did not increase over 0.65 V (data not included).

The reversible potentials corresponding to the following redox couples were indicated in Fig. 8 as a reference:

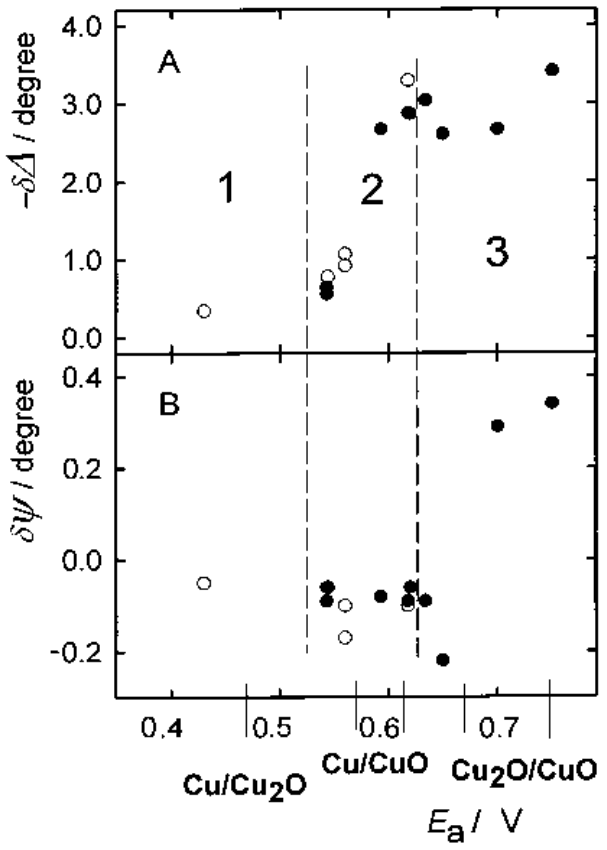

Fig. 8. Δ and Ψ measured after $t = 20$ min of potential holding at different anodic potentials E_a.(Procedure II, (○) v = 0.01 Vs^{-1}, (●) $v = 0.10$ V s^{-1}). In the abscissa the equilibrium potentials between different copper species are indicated. Regions 1, 2 and 3 limits are shown with dashed lines.

$$2Cu + H_2O = Cu_2O + 2H^+ + 2e^-$$
$$E = 0.471 - 0.059\,pH$$

$$Cu + H_2O = CuO + 2H^+ + 2e^-$$
$$E_1 = 0.570 - 0.059\,pH$$
$$E_2 = 0.609 - 0.059\,pH$$

$$Cu_2O + H_2O = 2CuO + 2H^+ + 2e^-$$
$$E_1 = 0.669 - 0.059\,pH$$
$$E_2 = 0.747 - 0.059\,pH$$

where E_1 corresponds to dehydrated and E_2 to the hydrated CuO, respectively [12].

3.2.4. Δ and Ψ during a potential scan in sol I and II. The ellipsometric and electrochemical responses obtained through procedure IV can be seen in Figs 9 and 10.

In sol I, Δ decreases markedly up to 0.53 V (Fig. 9). When the scan was reversed Δ attains a minimum at 0.52 V and then increases. Ψ decreases slowly during the anodic scan up to 0.50 V, returning to the initial value after the reverse scan. The voltammogram shows an anodic and a cathodic peak in the regions corresponding to the higher slopes in the Δ/E plot (0.6 V and 0.3 V, respectively).

In sol II, a significant decrease in Δ was observed at potentials about 50 mV more cathodic than in Fig. 9 reaching a minimum at 0.6 V (Fig. 10). As in the case of Fig. 9, Δ also reaches a minimum during the cathodic scan. However, Δ and Ψ values at the end of the experiment were not close to the initial values as in the case of sol I.

In the i against E curve a minimum at 0.5 V can be observed during the anodic scan (Fig. 10). The cathodic sweep shows a cathodic peak at 0.3 V similar to that observed in Fig. 9.

4. Discussion

It is well known that in sol Cu(II) is more stable than Cu(I) species due to the difference in energy of hydration [12]. In contrast, at the interface between CuO and Cu, in the absence of electric field, CuO tends to be reduced to Cu_2O (thermodynamically more stable) [12, 22]. Differential reflectometry shows that both Cu_2O and CuO are present on both sides near the equilibrium Cu_2O/CuO potential [13]. The spectra of these species are time dependent. After several hours an underlying film of Cu_2O was detected in a region were the Pourbaix diagram predicts that CuO (rather than Cu_2O) is the stable species.

The simulation of Cu_2O and CuO growth according to the optical indices reported in the literature is plotted in Fig. 11A. Typical data calculated at $\lambda = 546$ nm correspond to the average indices $n = 3.08$ −i 0.14 and $n = 2.66$ −i 0.58 for Cu_2O and CuO, respectively [14–18]. For Cu_2O layer thick-

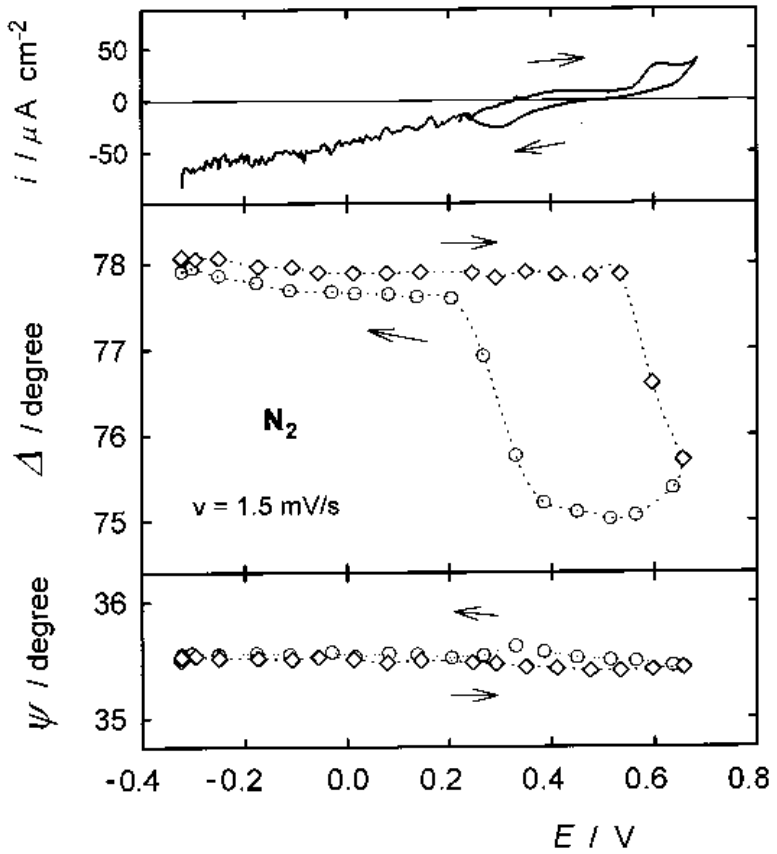

Fig. 9. Evolution of Δ, $\Psi$and the current density i against time during a cyclic scan between $E_c = -0.32$ V and $E_a = 0.68$ V, in N_2 sol. (◇) anodic scan, (○) cathodic scan.

nesses in the 0 nm< d < 4 nm range, changes in Δ of about 2.23 degree/nm and in Ψ of 0.25 degree/nm can be predicted. Similarly, in the case of CuO, Δ changes 1.73 degree/nm and Ψ −0.007 degree/nm.

At pH 9.2 additional redox couples which involve $Cu(OH)_2$ or other hydrated films make the description of the interface more complex.

4.1. *Processes taking place at the interface*

Optical and electrochemical results of copper in borax buffer saturated with N_2 or O_2 can be interpreted as a sequence of different interfacial processes including the formation of a barrier and a hydrated oxide layers, a dissolution process and a change in roughness.

4.1.1. Dissolution–precipitation. The increase in Ψ shown at E > 0.7 V in Figs 4, 5 and 8 and the irreversible change of Ψ shown in Fig 10 can be attributed to a dissolution precipitation process. Previous works [23, 24] show that Ψ increases because of the precipitation of a hydrated oxide layer making up the *outer part* of the *passivating layer* (o.p.p.l.). It was demonstrated [23] that $\delta\ \Psi$ can be taken as a measure of the total fraction of oxide that forms the o.p.p.l. The o.p.p.l. grows as a thick layer (i.e., 100–200 nm) of an initially very sparse material which becomes more compact as it retains increasing quantities of deposited species [23]. In those processes the interface develops as a film of constant thickness whose effective optical index n changes from a value similar to that of the electrolyte to higher values. These layers are relatively stable at cathodic potentials due to their high water content, which favours the faradaic hydrogen reaction in relation to oxide reduction [23, 24].

4.1.2. Barrier layer formation and cationic chemisorption. Results of Figs 2, 5 and 9 show the decrease in Δ with time which can be related to the growth of a Cu_2O layer [6–9].

Bulk samples of Cu_2O and CuO are defect semiconductors that are inherently p-type due to cation vacancies in the oxide lattice. According to the preparation method, conductivities vary greatly and variable internal stoichiometries can be expected [18–20]. Depending on the crystal structure, outer d electrons exhibit properties of: (i) localized electrons (having no Fermi surface), (ii) delocalized electrons (with a well defined Fermi surface), (iii) intermediate properties [21]. For cationic chemisorption on a p-type semiconductor, the Fermi level of the solid

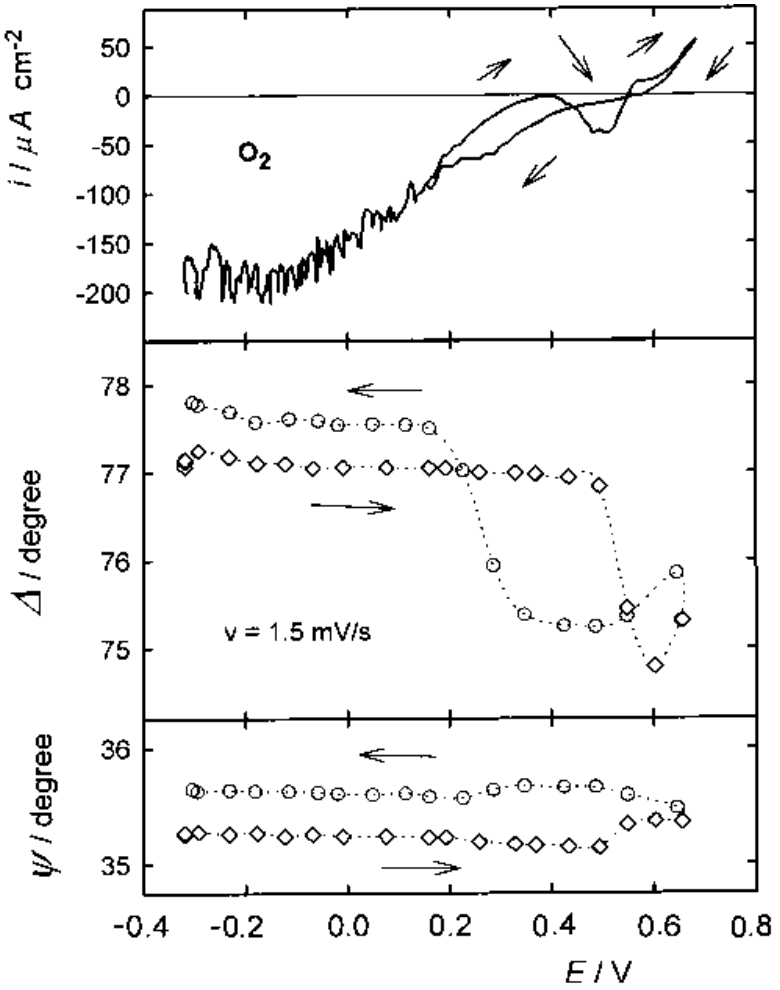

Fig. 10. As Fig. 9 but in O_2 saturated sol.

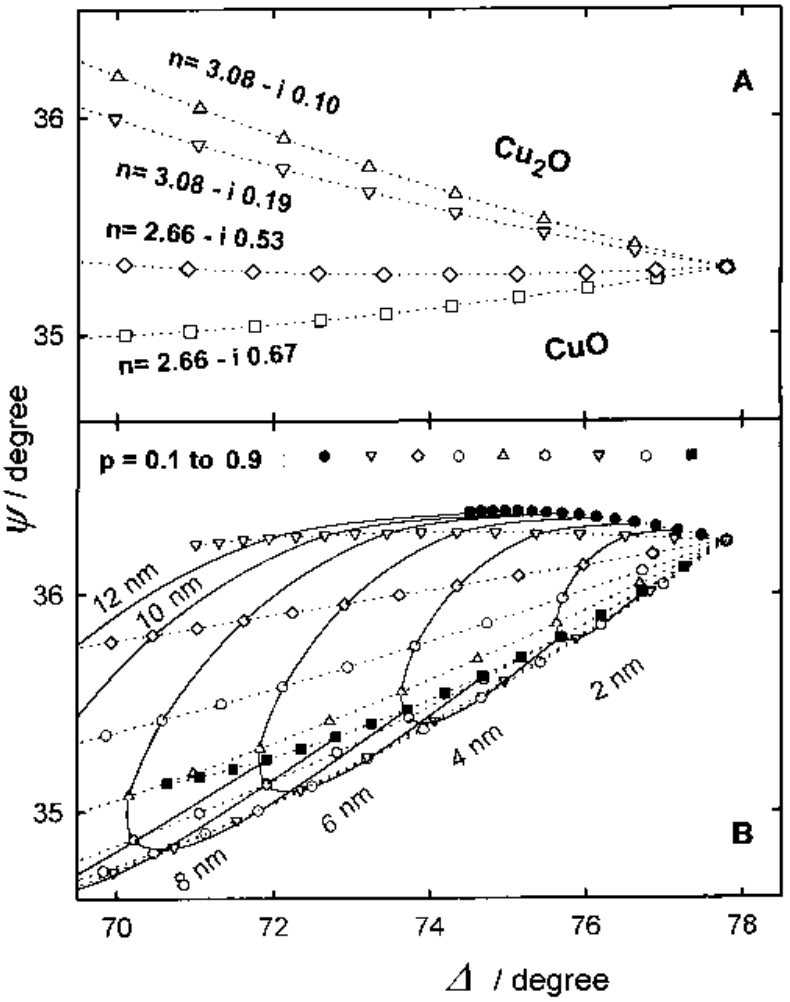

Fig. 11. Theoretical Δ and Ψ plots corresponding to: (A) Copper oxides films whose optical constants are indicated in the figure, for thickness increments $\delta d = 0.5$ nm. (B) Rough copper film for $\delta d = 1.0$ nm. The distinct symbols correspond to different volume fractions p of metal in the $0.1 < p < 0.9$ range, each 0.1.

gradually rises and, at equilibrium, equals the potential energy of the electrons in the adsorbate. A potential energy barrier is built up during the adsorption [22]. This process may change the optical constants corresponding to the bulk Cu_2O, increasing the value of the extinction coefficient k (Fig. 11A).

In the present case the adsorption of Cu(II) on the Cu_2O layer probably bends the semiconductor band deflecting the holes to the metal. In this way the growth of the *inner part* of the *passivating* Cu_2O layer (i.p.p.l.) stops (Figs 2 and 7) and the reduction of the Cu_2O species will occur at more anodic potentials (Fig. 6). When the dissolution process occurs, the concentration of adsorbed Cu(II) decreases and the growth of the i.p.p.l. is restored (Fig. 5).

4.1.3. Estimation of the roughness. To evaluate the possible change in roughness, Δ and Ψ were calculated employing effective optical indices predicted by the 'effective medium theory' [23–25]. Optical constants of the copper substrate $n = 0.9603$ –i 2.3937, of the electrolyte $n = 1.332$, a single homogeneous film and different metal volume /total volume ratios, p, ranging from 0.1 to 0.9 were assumed for this purpose. The Δ/Ψ plot forms a cone spreading to decreasing values of Δ, and constant or decreasing values of Ψ (Fig. 11B).

The $-\delta\Delta$ values corresponding to the surface after the reduction of the oxide formed during 24 h at E_{oc} are 6 degrees for N_2 sol and 5 degrees for O_2 sol, respectively (Fig. 1A and B, filled inverted triangles). Comparing Fig. 1B and 11B, a maximum thickness in the rough copper layer of about 9 nm can be predicted. A hydrated layer, which is not reduced remains on the surface. Consequently, the evaluation of the contributions of each layer to $-\delta\Delta$ and $\delta\Psi$ is complex.

4.2. *Potential regions*

The results of Figs 5 and 8 can be rationalized considering three potential regions: region I up to 0.56 V, region II from 0.56 V to 0.63 V and region III from 0.63 V to 0.75 V. The exact potential limits depend on the nature of the dissolved gas, perturbation programme and time.

Region I: It is characterized by the linear growth of a thin i.p.p.l. The film thickness, related to the Δ decrease (Fig. 11), increases slowly and linearly with time [6, 9].

Region II: It is characterized by parabolic growth of the i.p.p.l. The cathodic limit (~0.56 V) is lower if sol II is employed. As Δ and Ψ measured before film formation and after reduction are very similar (Fig. 4) roughness changes can be disregarded as in the case of region I.

The beginning of the reduction process, as well as the potentials of the reduction peaks, are more cathodic than those corresponding to oxide formation in region I (Figs 6 and 7). Thus, a more irreversible process or a higher ohmic drop owing to thicker oxide layers may be involved [26, 27].

The film thickness depends on the potential holding time (Fig. 8). The decrease in Δ ($-\delta\Delta$) associated with the film thickness is higher than in region I and proportional to the applied overpotential (Fig. 8).

In the gas phase the parabolic and the linear Δ/t law are interpreted as the contribution of volume diffusion and the interfacial reaction, respectively [28]. The parabolic law and the significant increase in thickness in region II may be related to an increase in the concentration of electron holes in the oxide layer at potentials more anodic than that corresponding to the Cu/CuO couple [12, 19, 29].

Region III: This region is characterized by a limiting film thickness (Fig. 7). Both $-\delta\Delta$ and QI reach maximum values in the cathodic limit of region III and then decrease for higher potentials (Figs 7 and 8). Ψ increases sharply between 0.65 and 0.70 V (Figs 5–8) and remains high after the reduction process. This change can be associated with a dissolution precipitation process. The QI/E plot agrees with reported data [2].

The oxide film formed in region III is more easily reduced at higher potentials than that formed in region II (Fig. 6). This shift in the reduction potential and the limiting film thickness suggest the existence of a chemisorption process previous to the electrochemical dissolution.

4.3. *Reaction pathways*

4.3.1. N_2 saturated sol. Comparing the results of Fig. 4 (0.70 V) with other previously reported data [2, 6, 9, 12, 23] it can be inferred that several processes contribute to the overall reaction: (i) the growth of the i.p.p.l. at the metal surface from the beginning up to $t = 3$ min; (ii) the growth of the o.p.p.l. from $t = 3$ to 15 min which remains on the surface without electroreducing during the cathodic scan. [The slope of the imaginary line (see arrows in Fig. 4) that goes from the Δ/Ψ points of the bare substrate to the first data at E_a ($t = 1$ min) and that between E_a ($t = 20$ min) and the reduced surface (filled inverted triangles) are similar, indicating the formation and reduction of the i.p.p.l.].

Accordingly, for long exposure periods at E_{oc} the structure of the interface obtained after cathodization at −0.32 V (Fig. 1, filled inverted triangles) may be described as the sum of two contributions: a copper rough layer and a o.p.p.l. [23].

4.3.2. O_2 saturated sol. Stable potentials of about 0.62 V, 0.64 V are attained in sol II after one or two hours at E_{oc} (region II). These lie between the equilibrium potentials corresponding to the redox couple Cu/CuO and Cu_2O/CuO [12] resulting in this case in a parabolic Δ/t law (Fig. 2B). In the case of sol I, E_{oc} is cathodic relative to the Cu/CuO equilibrium and the thickness increases linearly with the time.

Moliere *et al.* [1] explained some cooling efficiency losses of turbo generator stator by the accumulation of Cu oxide in the channels. Increasing the oxygen content up to 100 μgl dm^{-3} immediately reduces the release rate of the suspended particles. In the case of sol II the polarization of the surface in the presence of oxygen probably gives a flatter and more compact oxidation front and consequently controls the copper dissolution at low potentials in pure water.

The Δ/Ψ plots obtained at E_{oc} during 24 h (Fig. 1A and B) shows that $-\delta\Delta$ is higher (i.e., the i.p.p.l. is thicker) in sol II than in sol I. Conversely, after the reduction process, $-\delta\Delta$ is higher in sol I than in sol II. Assuming that the contribution of the o.p.p.l. only produces a change in Ψ [23] higher roughness of the copper substrate occurs in sol I after reduction. In this condition, owing to the different reactivity of the substrate crystalline faces [30, 31] and variations in the i.p.p.l. structure, higher roughness in the base metal may develop during oxide formation.

The higher E_{oc} in stagnant sol relative to stirred sol (Fig. 2A) may be explained by the increasing amount of chemisorbed Cu(II) caused by a more compact o.p.p.l. which hinders the dissolution process in stagnant sol. When the O_2 concentration was low, it was found [8] that Cu_2O was the stable phase. Thicker films found in pure deaerated water were attributed to a smaller tendency for the cuprous ions formed to be oxidized to the more soluble Cu(II) [8]. In contrast, in borax sol, O_2 increases the thickness of the i.p.p.l. and, probably, the amount of chemisorbed Cu(II) species (Fig. 2 and Fig. 11).

Figure 10 shows interesting features during the anodic scan which were not observed in Fig. 9: (i) a cathodic shift of 50 mV in the first decrease in Δ, (ii) an increase in Ψ at 0.5 V followed by an increase in Δ. The changes mentioned in (ii) remain after the reduction of the oxides showing that the surface condition has been modified (compare with Fig. 4). Consequently, in the presence of O_2 , regions II and III shift cathodically and the growth of the i.p.p.l. and dissolution precipitation processes occur at lower potentials.

The singular increase in the reduction rate of O_2, indicated by a maximum in the cathodic current at 0.5 V in Fig. 10, can be attributed to maximum chemisorption of Cu(II) in the limit of regions I and II.

4.4. *Further evidence of Cu(*II) chemisorption

Relationship between charge and thickness can be calculated assuming oxide densities of 6.0 g cm^{-3} and 6.4 g cm^{-3} for CuO and Cu_2O, respectively [7,18,20], resulting in 145.57 and 863.2 $\mu C\ nm^{-1}\ cm^{-2}$. These can be related to Δ values obtaining 841.44 μC $degree^{-1}\ cm^{-2}$ for CuO and 387.08 μC $degree^{-1}\ cm^{-2}$ for Cu_2O, respectively (Fig. 11).

A linear relationship between Q and $-\delta\Delta$ of 132.5 μC $degree^{-1}$ can be observed in Fig. 7. The electrode area being 0.4 cm^{-2} $Q/-\delta\Delta$ has a value of 331.25 μC $degree^{-1}\ cm^{-2}$. There is a good agreement between this value and that obtained from the Cu_2O density value. The increase in $Q/-\delta\Delta$ observed in Fig. 7 for $-\delta\ \Delta$ values higher than 2.5 degrees may be related to partial electrooxidation of the outer Cu_2O layer. This process is considered as the cathodic limit of region III and can be attributed to cationic chemisorption.

The linear increase of $\delta\Delta/t$ (Fig. 2) at constant E_{oc} potential (regions I and II), indicates that some redox or dynamic equilibria at the interface controls the E_{oc} behaviour independent of the film thickness. In contrast, if a simple i.p.p.l. were growing without chemisorption, E_{oc} would shift anodically with increase in thickness [29].

5. Conclusions

The sequence of i.p.p.l. and o.p.p.l. formation at the Cu/electrolyte interface was detected through optical and electrochemical experiments both at E_{oc} and controlled potential. There is competition between dissolution, electron hole formation and Cu(II) chemisorption processes which tend to control the growth and structure of the i.p.p.l. At high potentials the growth rate of the inner Cu_2O layer ($E > 0.53$ V, region II) and then the dissolution process ($E >$ 0.63 V, region III) are favoured and, consequently, the amount of chemisorbed Cu(II) decreases. The presence of O_2 shifts the potential limits of regions II and III cathodically.

Acknowledgements

This work was supported by the Consejo Nacional de Investigaciones Cientificas (CONICET) and the Comision de Investigaciones Cientificas de la Provincia de Buenos Aires (CIC) and Fundacion Antorchas. J. O. Z. and M. F. L. de M. are members of the Research Career of CIC and CONICET, respectively. The authors are grateful to M. Viera for her technical assistance.

References

[1] M. Moliere, Y. Verdier and C. Leymonie. *Corros Sci.* **30** (1990) 183.
[2] H. H. Strehblow and B. Titze, *Electrochim. Acta* **25** (1980) 839.
[3] M. F. L. de Mele, G. Brankevich and H. A. Videla, *Br. Corrosion J.* **24** (1989) 211.
[4] S. G. Gomez de Saravia, M. F. L. de Mele and H. A. Videla, *Corrosion* **46** (1990) 302.
[5] M. R. Viera, J. O. Zerbino and M. F. L. de Mele, Fifth Congr. Ibero Americano de Corrosion y Proteccion. Oct. (1995), Tenerife, Canarias, Spain.
[6] J. L. Ord, D. J. DeSmet and Z. Q. Huang, *J. Electrochem. Soc.* **134** (1987) 826.
[7] M. Yamashita, K. Omura and D. Hirayama, *Surf. Sci.* **96** (1980) 443.
[8] J. Kruger and J. P. Calvert, *J. Electrochem. Soc.* **111** (1964) 1038; *idem.* **108** (1961) 503.
[9] M. R. Gennero de Chialvo, J. O. Zerbino, S. L. Marchiano and A. J. Arvia, *J. Appl. Electrochem.* **16** (1986) 517.
[10] M. A. Ordal, L. L. Long, R. J. Bell, R. W. Alexander and C. A. Ward, *Appl. Optics.* **22** (1983) 1099.
[11] P. B. Johnson and R. W. Christy, *Phys. Rev. B* **11** (1975) 1315.
[12] M. Pourbaix, 'Atlas of Electrochem. Equilibria', Pergamon Press, Cebelcor, Brussels, (1966).
[13] C. W. Shanley, R. E. Hummel and E. D. Verink, *Corros. Sci.* **20** (1980) 481.
[14] P. C. Ladelfe, A. W. Czanderna and J. R. Biegen. *Thin Solid Films* **10** (1972) 483.
[15] V. F. Drobny and D. L. Pulfrey, *ibid.* **61** (1979) 89.
[16] B. Karlsson, C. G. Ribbing, A. Roos, E. Valkonen and T. Karlsson. *Physica Scripta* **25** (1982) 826.
[17] K. Bärwinkel and H. J. Schmidt, *Thin Solid Fims* **59** (1979) 373.
[18] H. Wieder and A. W. Czanderna, *J. Appl. Phys.* **37** (1966) 184.
[19] S. M. Wilheim, Y. Tanizawa, Chang-Yi Liu and N. Hackerman, *Corros. Sci.* **22** (1982) 791.
[20] D. R. Lide (Ed.), 'Handbook of Chemistry and Physics' 73rd ed, CRC Press (1992–93).
[21] J. B. Goodenough, 'Progress in Solid State Chemistry', vol. 5 (edited by H. Reiss) Pergamon Press (1971).
[22] J. M. Thomas and W. J. Thomas, 'Introduction to the Principles of Heterogeneous Catalysis', Academic Press, New York (1967). ch. 5, P. 258.
[23] O. A. Albani, L. M. Gassa, J. O. Zerbino, J. R. Vilche and A. J. Arvia, *Electrochim. Acta* **35** (1990) 1437.
[24] J. O. Zerbino, C. De Pauli, D. Posadas and A. J. Arvia, *J. Electroanal. Chem.* **330** (1982) 675.
[25] J. O. Zerbino, C. Perdriel and A. J. Arvia, *Thin Solid Films* **232** (1993) 63.
[26] N. R. Tacconi, J. O. Zerbino and A. J. Arvia, *J. Electroanal. Chem.* **79** (1977) 287.
[27] J. O. Zerbino, N. R. Tacconi, A. J. Calandra and A. J. Arvia, *J. Electrochem. Soc.* **476** (1977) 475.
[28] M. Rauh, P. Wißmann and M. Wolfel, *Thin Solid Films.* **228** (1993) 121; *ibid.* **233** (1993) 289.
[29] L. E. Eiselstein, B. C. Syrett, S. S. Wing and R. D. Caligari, *Corros. Sci.* **23** (1983) 223.
[30] M. Molière, Y. Verdier and C. Leymonie, *ibid* **30** (1990) 183.
[31] B. Pointu and P. Poncet, *Thin Solid Films* **79** (1981) 125.